The Rhythm of the Herd: Synchronization in a Network of Cows

Tuongvi Victoria Vo, Thomas Wang, Arjun Khurana, Joshua Dover

APMA1360 Spring 2025

Contents

1 Introduction

Mathematical modeling is a great approach for understanding complex patterns in natural and social systems. One fascinating area is synchronization, where individual parts of a system begin to coordinate their behavior. Synchronization occurs in many contexts. Even in typical farm settings, cows often lie down or stand up at the same time, showing subtle signs of social influence and group behavior. These patterns might seem simple, but they raise compelling questions about how local interactions between individuals can lead to group-wide coordination.

The paper "A Mathematical Model for the Dynamics and Synchronization of Cows" by Jie Sun, Erik M. Bollt, Mason A. Porter, and Marian S. Dawkins presents a mathematical framework for studying this type of behavior in cows. The authors introduce a model that describes each cow as a system that switches between three main behaviors: lying down, ruminating (resting state), and standing. The idea is that a cow's behavior is not just based on its internal rhythm, but also influenced by the behavior of nearby cows. This setup creates a system of interacting units that can lead to synchronized behavior across the group.

The model uses differential equations to represent each cow's internal dynamics, while coupling terms are added to reflect the influence of other cows. When coupling is strong, cows tend to behave more similarly over time; when it is weak, they act more independently. The authors explore different conditions to see how synchronization emerges, running simulations to show how group behavior depends on factors like coupling strength and network structure.

Our goal for this project is to take the ideas from this paper and make them easier to understand for a general audience. We want to explain the model clearly, simulate it ourselves, and interpret the results in a way that connects back to real-world behavior. We also experimented with a few of the authors' suggestions, such as changing some parameters or testing alternative setups, to see how that changes the outcome. We believe it adds an interesting layer to the project and helps us engage more deeply with the material.

By working through this model, we aim to highlight how mathematics can be used to explain familiar behaviors in animals and how simple interactions can lead to complex group dynamics. In the next sections, we will define the structure of the model, walk through our simulations and findings, and reflect on what we've learned about synchronization, both mathematically and biologically.

2 The single-cow model

This section introduces the mathematical model that describes the behavior of a single cow in isolation. The goal is to represent how internal physiological needs—hunger and the desire to rest—drive the cow's observable actions: eating, lying down, or standing. We define key state variables, present differential equations that govern their evolution, and explain the threshold-based switching rules that determine transitions between behaviors. By understanding this foundational model, we can later examine how coupling multiple cows together leads to synchronized behavior within a herd.

2.1 State Variables and Observation Modes

Each cow is modeled as a hybrid dynamical system consisting of continuous internal variables and a discrete observable behavior. The full state of the cow is defined as:

$$w = (x, y; \theta) \in [0, 1] \times [0, 1] \times \Theta,$$

where:

- x is the internal desire to eat (hunger),
- y is the internal desire to lie down (fatigue),
- $\theta \in \Theta = \{\mathcal{E}, \mathcal{R}, \mathcal{S}\}$ is the observable behavior.

The set of behaviors is defined as follows:

- $\mathcal{E}$ (Eating): The cow is actively eating.
- $\mathcal{R}$ (Ruminating): The cow is lying down (ruminating).
- $\mathcal{S}$ (Standing): The cow is standing but neither eating nor lying down.

2.2 Uncoupled Dynamics

The evolution of internal variables x and y follows behavior-specific differential equations:

Eating ($\theta = \mathcal{E}$):

$$\begin{cases} \dot{x} = -\alpha_2 x \\ \dot{y} = \beta_1 y \end{cases}$$

Ruminating ($\theta = \mathcal{R}$):

$$\begin{cases} \dot{x} = \alpha_1 x \\ \dot{y} = -\beta_2 y \end{cases}$$

Standing ($\theta = \mathcal{S}$):

$$\begin{cases} \dot{x} = \alpha_1 x \\ \dot{y} = \beta_1 y \end{cases}$$

All parameters α_1, α_2, β_1, and β_2 are assumed to be positive and reflect biologically motivated rates of change. Specifically, α_1 and α_2 represent the rate of increase and rate of decrease of hunger respectively. Similarly, β_1 and β_2 represent the rate of increase and rate of decrease of the desire to lie down.

This simple, linear model was chosen for ease of analysis, and although simple, still provides much to analyze.

2.2.1 Behavior Switching Rules

Behavior changes are triggered when x or y reaches a threshold:

- **Switch to Eating ($\theta = \mathcal{E}$):** if $\theta \in \{\mathcal{R}, \mathcal{S}\}$ and $x = 1$,
- **Switch to Ruminating ($\theta = \mathcal{R}$):** if $\theta \in \{\mathcal{E}, \mathcal{S}\}$, $x < 1$, and $y = 1$,
- **Switch to Standing ($\theta = \mathcal{S}$):** if $\theta \in \{\mathcal{E}, \mathcal{R}\}$ and either $x = \delta$ with $y < 1$, or $y = \delta$ with $x < 1$.

The constant δ is a small positive number that serves to eliminate the point $(0, 0)$, as well as the axes, from the domain of the model as the model begins to break down in those areas. We can interpret this as making sure the cow always wants to do something.

2.3 Discrete Dynamics and Poincaré Map

A problem in analyzing this model comes from the discontinuous changes in θ. To simplify the analysis, we consider only the discrete dynamics occurring at state transitions. These transitions are defined on a Poincare section to represent the main behaviors, eating and lying. This section is defined as the surface:

$$\Sigma = \{(x, y; \theta) \mid x = 1, \delta \leq y \leq 1, \theta = \mathcal{E}\} \cup \{(x, y; \theta) \mid \delta \leq x < 1, y = 1, \theta = \mathcal{R}\}$$

The full Poincare map on this section is represented by f.

Although this section is enough for analytical purposes, for convenience, we extend this domain to:

$$\Sigma' = \Sigma \cup \{(x, y; \theta) \mid x = \delta, \delta \leq y < 1\} \cup \{(x, y; \theta) \mid \delta \leq x < 1, y = \delta\}$$

The extended section includes the boundaries that represent $\mathcal{S}$. The map $g : \Sigma' \to \Sigma'$ governs how the state evolves between transitions. This discrete map allows us to analyze fixed points, periodic orbits, and long-term behavioral patterns.

2.3.1 Discrete Case Transitions in the Return Map g

The discrete return map g governs how the cow switches behaviors based on threshold crossings in hunger (x) and lying desire (y). Its explicit form can be derived directly from the single-cow equations.

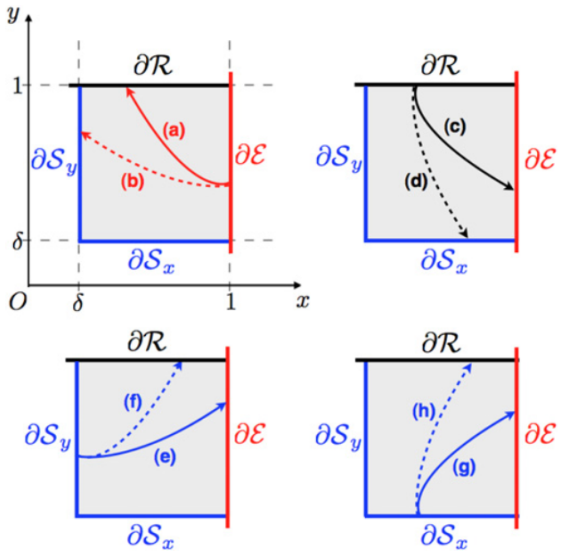

Figure 1: All possible switching transitions in the discrete return map g, adapted from the original model [2].

The rules for switching are summarized in Figure 1. To see where they come from, consider an initial point $w_0 = (1, y_0; \mathcal{E})$, i.e. a cow is currently eating. Since the equations that govern this state are simple first order equations, we can directly write down the solutions, assuming that $\theta = \mathcal{E}$ remains true,

$$\begin{cases} x(t) = e^{-\alpha_2 t} \\ y(t) = y_0 e^{\beta_1 t} \end{cases}$$

where $\delta < y_0 < 1$ and x_0 is necessarily equal to one. In order to discuss the switching dynamics, we need to know where the solutions intersect their switching boundaries. For $\mathcal{E}$, since, respectively, x and y decrease and increase monotonically, there are two possibilities for which boundary the solution intersects depending on the values of the parameters: $\partial\mathcal{R}$ and $\partial\mathcal{S}_y$.

In order to determine which boundary the solution will intersect, we need to determine what conditions lead to the solution intersecting at the corner, $(\delta, 1; \mathcal{R})$. Since $\partial\mathcal{R}$ has $y = 1$, we can easily determine the time that it takes the system to reach the boundary in the y-direction:

$$t = \frac{1}{\beta_1} \log \frac{1}{y_0}$$

Then, the x-variable has the same amount of time to move so we can solve for the position it will intersect $\partial\mathcal{R}$. Plugging in the expression for t into the solution for x,

$$x = y_0^{\alpha_2/\beta_1}$$

Requiring that $x = \delta$, we can solve for the value that y_0 must take in terms of δ,

$$y_0 = \delta^{\beta_1/\alpha_2}$$

This value represents a condition for the dynamics of g. If $y_0 \geq \delta^{\beta_1/\alpha_2}$, then the solution starting on $\partial\mathcal{E}$ will intersect $\partial\mathcal{R}$. If $y_0 < \delta^{\beta_1/\alpha_2}$, then the solution will intersect $\partial\mathcal{S}_y$.

For intersection at $\partial\mathcal{R}$ its straightforward to determine where the solution will intersect. In fact, we already solved for it. The solution will intersect $\partial\mathcal{R}$ at $(y_0^{\alpha_2/\beta_1}, 1; \mathcal{R})$. For intersection at $\partial\mathcal{S}_y$, we perform mostly the same calculations but starting by finding the time it takes for the x-variable to reach $x = \delta$.

$$t = \frac{1}{\alpha_2} \log \frac{1}{\delta}$$

Plugging in this quantity we find the point of intersection to be $(\delta, \delta^{\frac{\beta_1}{\alpha_2}} y_0; \mathcal{S})$.

Altogether, the dynamics of g for this starting condition look like:

$$g(x_0 = 1, \delta \leq y_0 \leq 1; \mathcal{E}) = \begin{cases} (y_0^{\frac{\alpha_2}{\beta_1}}, 1; \mathcal{R}) & \text{if } y_0 \geq \delta^{\frac{\beta_1}{\alpha_2}} \\ (\delta, \delta^{\frac{\beta_1}{\alpha_2}} y_0; \mathcal{S}) & \text{if } y_0 < \delta^{\frac{\beta_1}{\alpha_2}} \end{cases}$$

The rest of the possible switching dynamics are summarized below.

Case (a): Switching from Eating to Ruminating

$$g(x = 1, y; E) = \left(y^{\alpha_2/\beta_1}, 1; R\right) \quad \text{if } y \geq \delta^{\beta_1/\alpha_2}$$

The cow has reached maximum hunger while eating. Since its fatigue is sufficiently high, it switches to ruminating. The new hunger level depends on how much the desire to lie has grown during eating.

Case (b): Switching from Eating to Standing

$$g(x = 1, y; E) = \left(\delta, \delta^{-\beta_1/\alpha_2} y; S\right) \quad \text{if } y < \delta^{\beta_1/\alpha_2}$$

The cow is no longer hungry, but not tired enough to lie down. It moves to standing instead, with internal states updated according to inverse growth scaling.

Case (c): Switching from Ruminating to Eating

$$g(x, y = 1; R) = \left(1, x^{\beta_2/\alpha_1}; E\right) \quad \text{if } x \geq \delta^{\alpha_1/\beta_2}$$

The cow finishes lying down. If hunger has grown enough, it switches to eating. Fatigue is reset according to how much hunger has accumulated during rest.

Case (d): Switching from Ruminating to Standing

$$g(x, y = 1; R) = \left(\delta^{-\alpha_1/\beta_2} x, \delta; S\right) \quad \text{if } x < \delta^{\alpha_1/\beta_2}$$

The cow is not hungry enough yet to eat, so it stands. Hunger and fatigue are rescaled to reflect partial rest.

Case (e): Switching from Standing to Eating

$$g(x = \delta, y; S) = \left(1, \delta^{-\beta_1/\alpha_1} y; E\right) \quad \text{if } y \leq \delta^{\beta_1/\alpha_1}$$

From a standing position, the cow becomes hungry enough to eat again. Its desire to lie is not dominant, so it eats.

Case (f): Switching from Standing to Ruminating

$$g(x = \delta, y; S) = \left(y^{-\alpha_1/\beta_1} \delta, 1; R\right) \quad \text{if } y > \delta^{\beta_1/\alpha_1}$$

If fatigue is more urgent than hunger, the cow lies down instead. Hunger updates based on how long the cow remained standing.

Case (g): Switching from Standing to Eating

$$g(x, y = \delta; S) = \left(1, x^{-\beta_1/\alpha_1} \delta; E\right) \quad \text{if } x \geq \delta^{\alpha_1/\beta_1}$$

This is another case where eating wins. If hunger is strong while standing, the cow returns to eating.

Case (h): Switching from Standing to Ruminating

$$g(x, y = \delta; S) = \left(\delta^{-\alpha_1/\beta_1} x, 1; R\right) \quad \text{if } x < \delta^{\alpha_1/\beta_1}$$

Finally, if hunger is not dominant, the cow switches to lying down, with updated internal states.

These eight cases form the full piecewise definition of the return map g and determine how a single cow cycles between behaviors in response to internal thresholds. Each transition reflects biologically meaningful tradeoffs between hunger and fatigue.

2.4 Model Summary

This single-cow model captures the interplay between internal drives and external behavior using a hybrid dynamical system. The combination of continuous evolution and discrete switching yields a rich space of behavioral patterns, which will serve as the foundation for studying synchronization across multiple cows in the next section.

3 Analysis

Our analysis of the single-cow model will be limited to the discrete dynamics f on Σ. The dynamics of g on Σ', which are easily restricted to f, will merely be used as a tool. Specifically, we examine the unique fixed point of the system and investigate the existence of periodic orbits, particularly those with period 2. Throughout this analysis, we assume, without loss of generality, that the cow begins at the initial point $w_0 = (x_0, y_0; \theta_0) = (1, y_0; \mathcal{E})$ where $\delta \leq y_0 \leq 1$.

3.1 Fixed Points

For the single-cow model, there can only be a single fixed point on Σ given by $w_0 = (x_0, y_0; \theta) = (1, 1; \mathcal{E})$. This fixed point is asymptotically stable if and only if the following condition holds:

$$\frac{\alpha_2}{\alpha_1} \cdot \frac{\beta_2}{\beta_1} < 1$$

Note that, although the point $(0, 0)$ would be a fixed point, the Poincare map was defined in such a way that $(0, 0)$ was excluded from the domain. We then call $(0, 0)$ a *virtual* fixed point, one which the system will never reach, and so we exclude it in our analysis.

In order to prove this, we first need to introduce *flow*. Flow, for our single-cow model, refers to a solution to the system of equations at initial condition w_0 at time t_o, denoted $\phi(t - t_0, w_0)$. A key property of our system is that for any set of initial conditions, the flow of the single-cow model is always transverse to Σ, where $\Sigma = \partial\mathcal{E} \cup \partial\mathcal{R}$. Put simply, any flow of the single-cow equations will always intersect the boundary sharply. If the flow were tangent to the boundaries, switching states would be less clearly defined, posing problems for the model. Additionally, this implies some recurrence—i.e., all flows will eventually return to Σ.

We can use this fact to prove that no other point on Σ besides the corner can be a fixed point.

First, it is clear that any point that does not lie on Σ cannot be a fixed point, as all flows will always tend towards either $\partial\mathcal{R}$ or $\partial\mathcal{E}$ as shown above. Thus, any fixed point must lie on Σ.

Now, suppose that there is a fixed point at $(x_0, y_0; \theta) = (1, y_0; \mathcal{E})$. By definition, the flow starting at this point must return to it. But since it lies on Σ, and flows from Σ must be transverse to it, the trajectory must first rebound off of another boundary before returning to $\partial\mathcal{E}$.

If the flow intersects $\partial\mathcal{R}$, the state changes and the dynamics shift, yielding a nontrivial orbit. Since y increases at the same rate in both the $\mathcal{E}$ and $\mathcal{S}$ states (specifically, it increases exponentially at a rate determined by β_1), the flow must first rebound at $\partial\mathcal{S}_y$ before returning to $\partial\mathcal{E}$. Therefore, the flow beginning at $(1, y_0; \mathcal{E})$ will return to $\partial\mathcal{E}$ at a new point $(1, y_1; \mathcal{E})$. Since y increases monotonically, we conclude that $y_1 > y_0$, so the return point is different from the start. Thus, $(x_0, y_0; \theta)$ *cannot* be a fixed point—a contradiction. It is therefore impossible for any point $(1, y_0; \mathcal{E})$ for $\delta < y < 1$ to be a fixed point.

A similar argument can be applied to a hypothetical fixed point $(x_0, 1; \mathcal{R})$ with $\delta < x_0 < 1$, ruling out fixed points on $\partial\mathcal{R}$ as well.

In fact, since we see that any point on $\partial\mathcal{R}$ or $\partial\mathcal{E}$ tends in the positive x and y directions respectively, the only possible fixed point on Σ is at the corner: $(1, 1, \mathcal{E})$.

The stability of this point depends on the value of the parameters $\alpha_1, \alpha_2, \beta_1$ and β_2. If we want all trajectories to converge to $(1, 1)$ we require:

1. $\alpha_1 > \alpha_2$: When $\theta = \mathcal{E}$, the system moves left in x at a rate determined by α_2. When $\theta = \mathcal{R}$, it moves right in x at a rate determined by α_1. To settle into the fixed point, we require $\alpha_1 > \alpha_2$.

2. $\beta_1 > \beta_2$: Similarly, to ensure convergence in y, we require $\beta_1 > \beta_2$.

If these conditions are not met, the system tends away from the fixed point, leading instead to periodic orbits. We summarize the condition for asymptotic stability as:

$$\frac{\alpha_2}{\alpha_1} \cdot \frac{\beta_2}{\beta_1} < 1$$

A formal derivation of this condition will be seen in the next section, where we see that the fixed point is the orbit for which this condition holds.

3.2 Periodic Orbits

A key feature of the single-cow model is the many periodic orbits that arise. The simplest of these orbits on Σ are period-2, and can be categorized into four distinct cases, as depicted in the figure below:

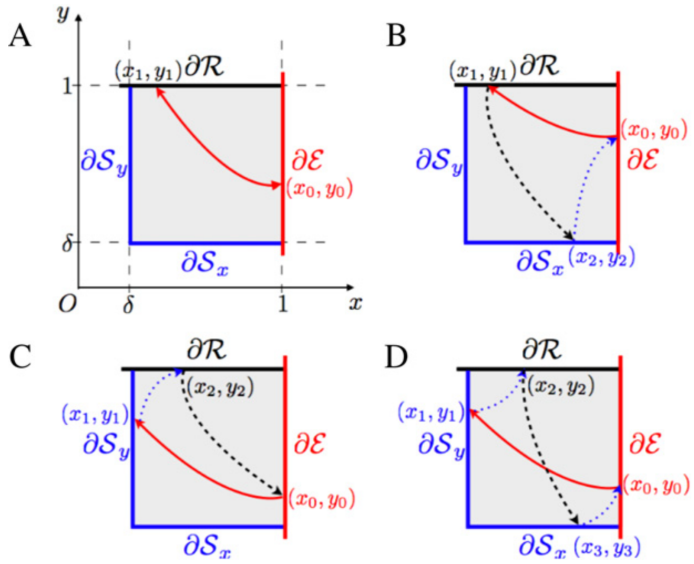

Figure 2: Graphical depiction of all possible period-2 orbits on Σ, split into four broad cases [2].

Note, that some of the orbits described are actually higher period on Σ', but reduce to period-2 when restricted to dynamics only on Σ.

3.2.1 Case A

The simplest of these cases is the one in which the orbit merely bounces between $\partial\mathcal{E}$ and $\partial\mathcal{R}$, returning to the same point each time. In order for this to occur, the following condition must be satisfied:

$$\frac{\alpha_2}{\alpha_1} \cdot \frac{\beta_2}{\beta_1} = 1$$

This mirrors the condition for marginal stability at the fixed point. If this condition holds, then after rebounding at $(x_1, y_1; \mathcal{R})$, the flow originating from (x_0, y_0) will always return to (x_0, y_0). We discuss how this condition arises.

To start, we observe what happens when we continually apply the map f to some initial condition. Without loss of generality, we assume the initial point lies somewhere on $\partial\mathcal{E}$: $w_0 = (x_0, y_0; \theta_0) = (1, y_0; \mathcal{E})$, where $\delta < y_0 < 1$. Applying f (or g) to w_0 and using the switching dynamics defined earlier, the next point on $\partial\mathcal{R}$ is:

$$w_1 = f(w_0) = g(w_0) = (x_1, y_1; \theta_1) = (y_0^{\frac{\alpha_2}{\beta_1}}, 1; \mathcal{R})$$

where $y_0 \geq \delta^{\frac{\beta_1}{\alpha_2}}$. This last condition ensures that the flow coming from w_0 intersects $\partial\mathcal{R}$ rather than $\partial\mathcal{S}_y$ (The case where $y_0 < \delta^{\frac{\beta_1}{\alpha_2}}$ will be examined in Case C).

Now, applying f to w_1, the next point on $\partial\mathcal{E}$ is:

$$w_2 = f(w_1) = (x_2, y_2; \mathcal{E}) = (1, x_1^{\frac{\beta_2}{\alpha_1}}; \mathcal{E})$$

where $x_1 \geq \delta^{\frac{\alpha_1}{\beta_2}}$. Recall that $x_1 = y_0^{\frac{\alpha_2}{\beta_1}}$. Substituting the expression for x_1, we get:

$$w_2 = (1, y_0^{\frac{\alpha_2\beta_2}{\alpha_1\beta_1}}; \mathcal{E})$$

To return to the original point, we must have $w_2 = w_0$, which implies:

$$\frac{\alpha_2}{\alpha_1} \cdot \frac{\beta_2}{\beta_1} = 1$$

We also restrict y_0 to $\delta^{\beta_1/\alpha_2} < y_0 < 1$ and less than one. If $\alpha_2 > \beta_1$, this remains the strongest lower bound on y_0 (since $0 < \delta < 1$, and an exponent less than 1 increases the value). However, if $\alpha_2 \leq \beta_1$, then the original $\delta < y < 1$ bound is stronger.

All orbits of this nature are stable, as small perturbations will inevitably settle into this type of orbit, so long as the condition on the parameters holds. Moreover, because the value of y_0 is not uniquely determined, there are infinitely many such orbits satisfying the condition.

3.2.2 Case B

In this case, the orbit, on Σ', is actually period-3, but reduces to period-2 when restricted to Σ. Orbits of these type must satisfy the following conditions:

$$\frac{\alpha_2}{\alpha_1} \cdot \frac{\beta_2}{\beta_1} > 1$$

$$\frac{1}{\alpha_1} + \frac{1}{\alpha_2} \geq \frac{1}{\beta_1} + \frac{1}{\beta_2},$$

so long as $\beta_1 < \alpha_2$. Broadly, orbits of this type first intersect $\partial\mathcal{R}$. Instead of re-intersecting $\partial\mathcal{E}$, the flow then intersects $\partial\mathcal{S}_x$ before returning to the starting point.

These conditions arise analytically from the same procedure used in Case A. However, when $\theta = \mathcal{S}$, we cannot apply f but must instead apply g.

As before, for $w_0 = (1, y_0; \mathcal{E})$. Applying f (or g) leads to a point on $\partial\mathcal{R}$ defined as:

$$w_1 = f(w_0) = g(w_0) = (x_1, y_1; \theta_1) = (y_0^{\frac{\alpha_2}{\beta_1}}, 1; \mathcal{R})$$

where $y_0 \geq \delta^{\frac{\beta_1}{\alpha_2}}$. Since the next point must lie on $\partial\mathcal{S}_x$, we apply g to w_1:

$$w_2 = g(w_1) = (x_2, y_2; \theta_2) = (\delta^{-\frac{\alpha_1}{\beta_2}} x_1, \delta; \mathcal{S}),$$

where $x_1 < \delta^{\frac{\alpha_1}{\beta_2}}$.
Finally, returning to $\partial\mathcal{E}$:

$$w_3 = f(w_2) = g(w_2) = (x_3, y_3; \theta_3) = (1, x_2^{-\frac{\beta_1}{\alpha_1}}\delta; \mathcal{E})$$

Substituting $x_1 = y_0^{\frac{\alpha_2}{\beta_1}}$, we get:

$$y_3 = x_2^{-\frac{\beta_1}{\alpha_1}}\delta = x_1^{-\frac{\beta_1}{\alpha_1}}\delta^{\frac{\beta_1}{\beta_2}+1} = y_0^{-\frac{\alpha_2}{\alpha_1}}\delta^{\frac{\beta_1}{\beta_2}+1}.$$

To return to the starting point, we require $y_3 = y_0$, and solve for y_0, which gives:

$$y_0 = \delta^{\frac{1+\frac{\beta_1}{\beta_2}}{1+\frac{\alpha_2}{\alpha_1}}}$$

This defines the *only* initial condition that results in this type of periodic orbit for a fixed set of parameters. To ensure the orbit exists and does not reduce to Case A or the fixed point, we again require:

$$\frac{\alpha_2}{\alpha_1} \cdot \frac{\beta_2}{\beta_1} > 1$$

If this quantity were to be equal to one, the orbit would settle into a stable period-2 orbit from case A. If it were less than one, it would settle into the fixed point. For now, we take this as given, but will see where it comes from in a later case.

Furthermore, we can use the bounds on y_0 to derive the other condition. Assuming $\alpha_2 > \beta_1$, the strongest restriction on y_0 is $y_0 \geq \delta^{\frac{\beta_1}{\alpha_2}}$. From this fact, we can extract the other condition. Since y_0 has a defined value, we can rewrite the restriction as

$$\delta^{\frac{1+\frac{\beta_1}{\beta_2}}{1+\frac{\alpha_2}{\alpha_1}}} \geq \delta^{\frac{\beta_1}{\alpha_2}}$$

Taking the logarithm of both sides, and simplifying the fraction on the left hand side, we reach:

$$\frac{\alpha_1(\beta_1+\beta_2)}{\beta_2(\alpha_1+\alpha_2)} \leq \frac{\beta_1}{\alpha_2}$$

Note, in order to bring down the exponents, we take the logarithm base δ. However, since $0 < \delta < 1$, the logarithm base δ is strictly decreasing, and so the direction of the inequality must be flipped. Further simplifying, we reach the original condition:

$$\frac{1}{\beta_1} + \frac{1}{\beta_2} \leq \frac{1}{\alpha_1} + \frac{1}{\alpha_2}$$

If $\alpha_2 < \beta_1$, then this condition is not necessary, and the orbit still exists, with looser bounds on y_0.

Lastly, these orbits are asymptotically stable. We can see how this condition arises by observing what happens when we iterate f on w_0, n times, and observe the behavior as n approaches infinity. As we saw from the first cycle, $y_3 = y_0^{-\frac{\alpha_2}{\alpha_1}}\delta^{\frac{\beta_1}{\beta_2}+1}$. Ignoring the δ term, we see that the y_0 term, as we continue to iterate over the whole cycle, is raised to another power of the term α_2/α_1 each go-around. By definition of asymptotic stability, if we continue this as n approaches infinity, the whole term will eventually reduce down to w_0 so long as we require that $\frac{\alpha_2}{\alpha_1} < 1$, so the term does not blow up as we continue to iterate. We can therefore state that periodic orbits of this type are asymptotically stable only if $\alpha_2 < \alpha_1$. In the case where the $\alpha_1 = \alpha_2$, the orbit is not asymptotically stable.

3.2.3 Case C

Analytically, case C is very similar to case B. The main difference is that the flow, originating from a point on $\partial\mathcal{E}$, now intersects $\partial\mathcal{S}_y$ before intersecting $\partial\mathcal{R}$ and returning to $\partial\mathcal{E}$. This has the effect of slightly modifying the conditions for this orbit to emerge. Orbits of this type must satisfy:

$$\frac{\alpha_2}{\alpha_1} \cdot \frac{\beta_2}{\beta_1} > 1$$

$$\frac{1}{\alpha_1} + \frac{1}{\alpha_2} < \frac{1}{\beta_1} + \frac{1}{\beta_2}$$

so long as $\alpha_2 > \beta_1$. Unlike Case B, this last inequality is necessary here.

These conditions are derived in similar fashion to case B. From a point w_0 on $\partial\mathcal{E}$, the flow first intersects $\partial\mathcal{S}_y$ at a point w_1. Following the dynamics laid out in the previous section, we get:

$$w_1 = g(w_0) = (\delta, \delta^{-\frac{\beta_1}{\alpha_2}} y_0; \mathcal{S})$$

where $y_0 < \delta^{\frac{\beta_1}{\alpha_2}}$, since otherwise the exponent would not increase the value (as $\delta < 1$). Hence, we require $\delta < y_0 < \delta^{\frac{\beta_1}{\alpha_2}}$.

The next point must lie on $\partial\mathcal{R}$:

$$w_2 = g(w_1) = (y_1^{-\frac{\alpha_1}{\beta_1}} \delta, 1; \mathcal{R})$$

where $y_1 > \delta^{\frac{\beta_1}{\alpha_1}}$. Lastly, returning to $\partial\mathcal{E}$,

$$w_3 = g(w_2) = (1, x_2^{\frac{\beta_2}{\alpha_1}}; \mathcal{E})$$

where $x_2 > \delta^{\frac{\alpha_1}{\beta_2}}$. Since we require that $w_3 = w_0$, we can solve for y_0 in a similar way to case B:

$$y_3 = x_2^{\frac{\beta_2}{\alpha_1}} = y_1^{-\frac{\beta_2}{\beta_1}} \delta^{\frac{\beta_2}{\alpha_1}} = y_0^{-\frac{\beta_2}{\beta_1}} \delta^{\frac{\beta_2}{\alpha_2} + \frac{\beta_2}{\alpha_1}}.$$

Solving for y_0 leads to:

$$y_0 = \delta^{\frac{\frac{1}{\alpha_1} + \frac{1}{\alpha_2}}{\frac{1}{\beta_1} + \frac{1}{\beta_2}}}$$

As in case B, the value of y_0 is fixed. Therefore, only one of these orbits can exist for a fixed set of parameters. Using the restrictions we placed on y_0, ($\delta < y_0 < \delta^{\frac{\beta_1}{\alpha_2}}$), as well as our new definition for y_0, we can derive further restrictions on the parameters. For the lower bound, after lowering the exponents (and flipping the inequality just as before), it is clear that:

$$1 > \frac{\frac{1}{\alpha_1} + \frac{1}{\alpha_2}}{\frac{1}{\beta_1} + \frac{1}{\beta_2}}$$

from which the condition cited above is readily drawn. From the upper limit, we derive explicitly the condition that,

$$\frac{\alpha_2}{\alpha_1} \cdot \frac{\beta_2}{\beta_1} > 1$$

These orbits are asymptotically stable so long as $\beta_2 < \beta_1$. The logic to reach this conclusion is identical to that used in case B, only the role of eating and lying down is reversed.

3.2.4 Case D

Case D is a combination of cases B and C. Starting from a point on $\partial\mathcal{E}$, the flow first intersects $\partial\mathcal{S}_y$, then $\partial\mathcal{R}$, and lastly $\partial\mathcal{S}_x$ before returning to $\partial\mathcal{E}$. Orbits of this type must satisfy:

$$\frac{\alpha_2}{\alpha_1} \cdot \frac{\beta_2}{\beta_1} > 1$$

$$\frac{1}{\alpha_1} + \frac{1}{\alpha_2} = \frac{1}{\beta_1} + \frac{1}{\beta_2}$$

The analysis of these orbits proceeds as usual, except now, the flow must cycle through four points in order to make one cycle. The first two points are identical to case C. For $w_0 = (1, y_0, \mathcal{E})$,

$$w_1 = g(w_0) = (\delta, \delta^{-\frac{\beta_1}{\alpha_2}} y_0; \mathcal{S})$$

where $y_0 < \delta^{\frac{\beta_1}{\alpha_2}}$. This condition once again necessitates that $\alpha_2 > \beta_1$. And,

$$w_2 = g(w_1) = (y_1^{-\frac{\alpha_1}{\beta_1}} \delta, 1; \mathcal{R})$$

where $y_1 > \delta^{\frac{\beta_1}{\alpha_1}}$. Next, unique to case D, the flow must first intersect $\mathcal{S}_x$ before returning. Referring to the dynamics of g on Σ',

$$w_3 = g(w_2) = (\delta^{-\frac{\alpha_1}{\beta_2}} x_2, \delta; \mathcal{S})$$

where $x_2 < \delta^{\frac{\alpha_1}{\beta_2}}$. Lastly, returning to $\partial\mathcal{E}$,

$$w_4 = g(w_3) = (1, x_3^{-\frac{\beta_1}{\alpha_1}} \delta; \mathcal{E})$$

where $x_3 \geq \delta^{\frac{\alpha_1}{\beta_1}}$. Evaluating as usual, we see that:

$$y_4 = x_3^{-\frac{\beta_1}{\alpha_1}} \delta = x_2^{-\frac{\beta_1}{\alpha_1}} \delta^{\frac{\beta_1}{\beta_2}+1} = y_1 \delta^{-\frac{\beta_1}{\alpha_1}+\frac{\beta_1}{\beta_2}+1} = y_0 \delta^{-\frac{\beta_1}{\alpha_2}-\frac{\beta_1}{\alpha_1}+\frac{\beta_1}{\beta_2}+1}$$

Requiring that $y_4 = y_0$ leads to:

$$0 = -\frac{\beta_1}{\alpha_2} - \frac{\beta_1}{\alpha_1} + \frac{\beta_1}{\beta_2} + 1 \implies \frac{1}{\alpha_1} + \frac{1}{\alpha_2} = \frac{1}{\beta_1} + \frac{1}{\beta_2}$$

Similar to case A, these conditions yield infinitely many stable orbits that satisfy them, so long as $\delta < y_0 < \delta^{\frac{\beta_1}{\alpha_2}}$.

Case D is a special boundary case between B and C, occurring precisely when the sums of reciprocals of α_1 and α_2 and β_1 and β_2 are equal. Since the solutions evolve exponentially, these reciprocals can be interpreted as time constants—rough measures of how long the cow spends in each behavioral state. The condition can then be interpreted as the cow spending equal amounts of time changing its level of hunger (i.e. eating) as changing its desire to lie down. The other cases can be considered as an imbalance of these two time-scales, where the desire to eat dominates in case B, and the desire to lie down dominates in case C.

4 Coupled Cows and Synchronization

This section extends the single-cow model to explore how collective behavior can emerge from local interactions. Synchronization, a central concept in coupled dynamical systems, provides a framework for understanding how individual agents with limited communication can coordinate their behavior. In this biologically grounded setting, we examine how decentralized rules and partial information can lead to group-level coherence. Specifically, we test whether a small herd of cows, each following the same internal dynamics, can synchronize transitions between observable states when weakly coupled through visible behaviors like eating and resting.

4.1 Model Overview

We extend the single-cow model to simulate a group of cows that interact with one another through observable behavior. Each cow continues to follow internal dynamics based on two physiological drives: hunger (x) and tiredness (y). Transitions between observable states—Eating ($\mathcal{E}$), Resting ($\mathcal{R}$), and Standing ($\mathcal{S}$)—are triggered when x or y cross predefined thresholds, as in the uncoupled model.

To simulate the herd, we treat each cow as a node in a network. While each cow still updates its internal variables based on its own behavior, it now also responds to the behavior of neighboring cows. For instance, a cow may become hungrier when others around it are eating, or more tired when it observes others resting. These assumptions are biologically plausible and supported by observations of animal behavior [2].

We model these interactions by introducing coupling terms into the differential equations. The internal dynamics for cow i become:

$$\dot{x}_i = \alpha^{(i)}(\theta_i)x_i + \frac{\sigma_x}{k_i}\sum_{j=1}^{n} a_{ij}\chi_{\mathcal{E}}(\theta_j)x_i, \quad \dot{y}_i = \beta^{(i)}(\theta_i)y_i + \frac{\sigma_y}{k_i}\sum_{j=1}^{n} a_{ij}\chi_{\mathcal{R}}(\theta_j)y_i$$

Here, $\alpha^{(i)}(\theta_i)$ and $\beta^{(i)}(\theta_i)$ are behavior-dependent growth or decay rates. These generalize the single-cow coefficients (α_1, α_2, β_1, β_2) by allowing each cow i to have slightly different parameters depending on its current state θ_i. For example, when cow i is eating ($\theta_i = \mathcal{E}$), we set $\alpha^{(i)}(\theta_i) = -\alpha_2^{(i)}$ and $\beta^{(i)}(\theta_i) = \beta_1^{(i)}$, mirroring the dynamics from the uncoupled case.

The indicator functions $\chi_{\mathcal{E}}(\theta_j)$ and $\chi_{\mathcal{R}}(\theta_j)$ return 1 if neighbor j is currently eating or resting, respectively. The adjacency matrix a_{ij} defines the network structure, with $a_{ij} = 1$ indicating that cow i observes cow j, and 0 otherwise. The degree $k_i = \sum_j a_{ij}$ ensures that the influence of neighbors is normalized across different connectivity levels. The coupling parameters σ_x and σ_y control how sensitive a cow is to its neighbors' eating and resting behaviors. This framework allows us to study how synchronization might emerge from local interactions: cows do not coordinate explicitly, but may gradually align their behavior through mutual influence.

4.2 Measuring Synchrony

To evaluate whether cows are synchronized, we compare the timing of transitions into the Eating ($\mathcal{E}$) and Resting ($\mathcal{R}$) states. For each cow i, we record the time steps $\tau^{(i)}$ and $\kappa^{(i)}$ when it enters these states. Synchrony is measured by comparing these sequences across cow pairs.

For cows i and j, we compute the average absolute difference between their eating times and between their resting times, allowing integer shifts of up to 10 steps. This yields two values, $\Delta_{ij}^{\mathcal{E}}$ and $\Delta_{ij}^{\mathcal{R}}$, which quantify alignment in eating and resting behavior, respectively.

Averaging over all pairs (including self-pairs, for which the synchrony error is zero), we define:

$$\Delta^{\mathcal{E}} = \frac{1}{n^2}\sum_{i,j}\Delta^{\mathcal{E}}_{ij}, \quad \Delta^{\mathcal{R}} = \frac{1}{n^2}\sum_{i,j}\Delta^{\mathcal{R}}_{ij}, \quad \Delta = \Delta^{\mathcal{E}} + \Delta^{\mathcal{R}}.$$

Smaller values of Δ indicate higher synchronization across the herd.

4.3 Two-Cow Results

To understand synchronization in the simplest setting, we simulated a pair of cows with slightly different parameters, following the method used in [2]. Each cow starts in the Eating state and switches between Eating, Resting, and Standing according to its internal hunger (x) and tiredness (y). The cows are fully connected, meaning each observes the other's behavior.

To test whether coupling could promote synchronization, we introduced slight parameter mismatches around shared baseline values:

$$\alpha_1^{(1,2)} = 0.05 \pm \epsilon, \qquad \alpha_2^{(1,2)} = 0.10 \pm \epsilon,$$
$$\beta_1^{(1,2)} = 0.05 \pm \epsilon, \qquad \beta_2^{(1,2)} = 0.125 \pm \epsilon,$$

where $\epsilon \in \{0.001, 0.01\}$ indicates the strength of mismatch. The switching threshold was fixed at $\delta = 0.25$.

Simulations ran for 30,000 time steps using Euler's method with a step size of 0.5, totaling 15,000 time units. At each step, we recorded the observable state and measured synchronization by comparing when the cows transitioned into Eating and Resting. To reduce noise, each condition was repeated across 50 trials. Figure 3 shows the resulting trial-averaged synchronization error, plotted against coupling strength σ for two levels of parameter mismatch: $\epsilon = 0.001$ and $\epsilon = 0.01$. Increasing σ improves alignment in state transitions across both mismatch levels. With the smaller mismatch ($\epsilon = 0.001$), eating and resting behaviors show low average error at higher coupling values, though variability remains high at lower coupling. When the mismatch is larger ($\epsilon = 0.01$), average errors are consistently higher, but the trend is smoother and variability appears smaller due to the broader scale of the plot. Overall, coupling promotes synchronization in both eating and resting dynamics, though fluctuations persist.

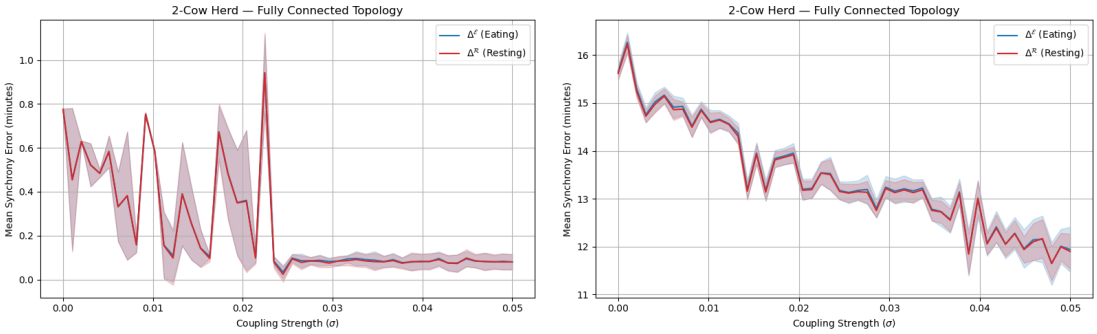

Figure 3: Synchronization error for two cows with parameter mismatch $\epsilon = 0.001$ (left) and $\epsilon = 0.01$ (right), plotted against coupling strength σ.

To visualize how this synchronization plays out over time, we plotted the observable states for a single trial with parameter mismatch $\epsilon = 0.001$ (Figure 4). Without coupling, the cows quickly diverge and transition at different times. When coupling is applied, they gradually align their

behaviors, despite parameter differences. These results support the conclusion that even weak interaction can promote shared rhythms in small systems.

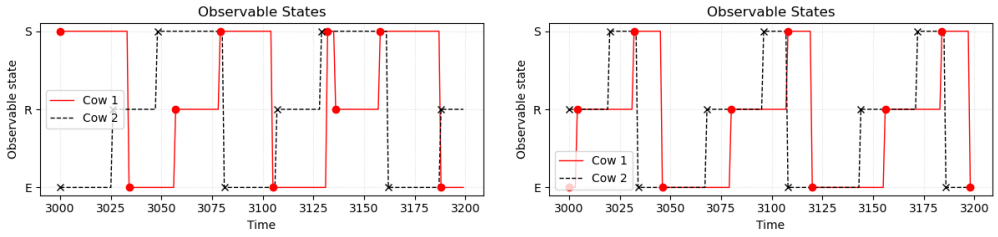

Figure 4: Observable states for two cows with parameter mismatch $\epsilon = 0.001$. Left: Uncoupled ($\sigma_x = \sigma_y = 0$). Right: Coupled ($\sigma_x = \sigma_y = 0.045$).

4.4 Synchronization in Larger Herds

To study how synchronization scales with herd size and network connectivity, we simulated groups of 10 cows with independently perturbed parameters. Each cow's parameters were drawn by adding uniform noise (bounded by 10^{-3} per parameter) to a shared baseline:

$$\alpha_1 = 0.05, \quad \alpha_2 = 0.10, \quad \beta_1 = 0.05, \quad \beta_2 = 0.125.$$

These perturbations were sampled independently for each cow and for each trial, introducing random heterogeneity across the herd. All cows began in the Eating state, with hunger initialized at $x = 1$ and tiredness y drawn uniformly from $[\delta, 1.0]$. The switching threshold was fixed at $\delta = 0.25$.

Simulations ran for 30,000 time steps using Euler integration with a step size of 0.5. At each step, we recorded the observable state of each cow and computed synchronization errors based on when cows transitioned into Eating and Resting. Synchrony metrics were averaged over 50 trials per condition; shaded error bands represent one standard deviation.

We tested four network topologies to evaluate the effect of connectivity:

- **Fully Connected**: Each cow observes all others (maximal connectivity).
- **2D Grid**: Cows are arranged on a 2×5 lattice and interact with immediate horizontal and vertical neighbors as depicted in Figure 6.
- **Random Network (sparse)**: Each edge is included with probability $p = 0.3$, creating irregular sparse networks.
- **Random Network (dense)**: Edges included with probability $p = 0.75$, yielding denser graphs.

Random networks were regenerated each trial, along with new cow parameters. Grid and fully connected topologies remained fixed across trials.

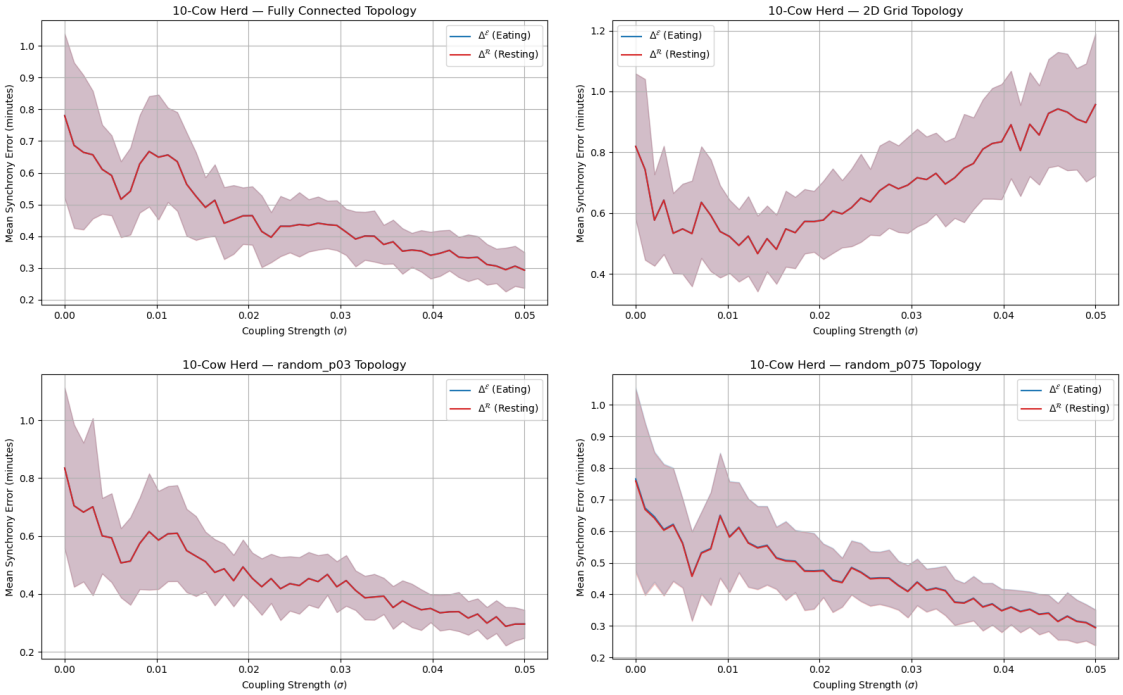

Figure 5: Synchronization error versus coupling strength σ for four network topologies. Fully connected and 2D grid (top), sparse and dense random networks (bottom).

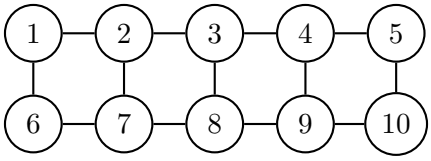

Figure 6: 2D grid topology used in 10-cow simulations. Each node represents a cow connected to its immediate horizontal and vertical neighbors.

As shown in Figure 5, both coupling strength and network structure have a substantial impact on synchronization. The fully connected network achieves the lowest resting synchronization error, with values decreasing from approximately 0.78 to 0.29 as σ increases. The dense random network ($p = 0.75$) performs nearly as well, indicating that high connectivity, whether fully structured or randomly distributed, strongly supports coordination. The sparse random network ($p = 0.3$) and the 2D grid topology both exhibit weaker synchrony, particularly at low to moderate coupling strengths. Notably, the grid shows the highest minimum resting error ($\Delta^{\mathcal{R}} \approx 0.47$), underscoring the limitations of strictly local interactions. These findings reinforce the conclusion that global or dense connectivity promotes emergent synchronization, while sparse or locally constrained networks inhibit collective alignment.

4.5 Synchronization in Walking Herds

Real cows do not exist in fixed graphs, but rather wander about 2D Euclidean space. To incorporate this into the model outlined by Sun et al., we construct a dynamic network topology based on a simple simulation of cow movement.

We place our cows in a "pasture" comprising positions in $[0, 1]^2$. Each cow is assigned two additional parameters: a walking speed γ and a vision radius ρ. We measure synchrony through simulation using Euler integration as stated above, with two additional changes:

1. At each time step, cows in state $\mathcal{S}$ "walk" one step; i.e. their positions in the pasture are perturbed by a value selected from a uniform distribution along $[-\gamma, \gamma]$.

2. The adjacency matrix for coupling is constructed using proximity in the pasture. More specifically, two cows are coupled if the Euclidean distance between them is less than ρ.

In these experiments, we do not vary ρ and γ between cows within a single herd. Doing so would be consistent with this model, but notably would result in asymmetric coupling graphs.

We bind the other cow parameters to the same values as the large herd synchronization of the previous section, and we proceed to simulate herds of 10 cows averaging over 20 trials.

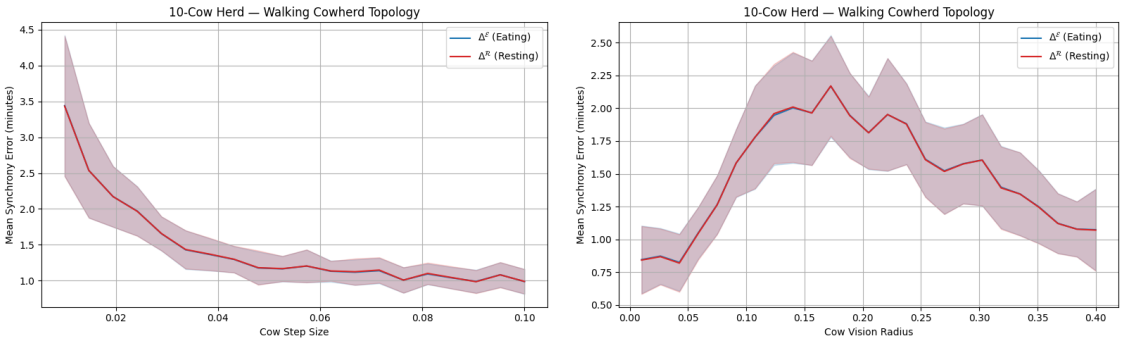

Figure 7: Synchronization error versus cow pasture parameters.

Figure 7 comes from two sets of simulations. In the left plot, we vary γ while fixing $\rho = 0.2$, allowing us to conclude that increased movement among cows increases synchrony. In the right plot, we vary ρ while fixing $\gamma = 0.02$, which seems to indicate that synchrony is bimodal in vision radius (*n.b.* decreased synchrony error values in these plots indicate increased synchrony, effectively inverting the plots vertically.)

Figure 8 shows how synchrony varies as we vary both γ and ρ.

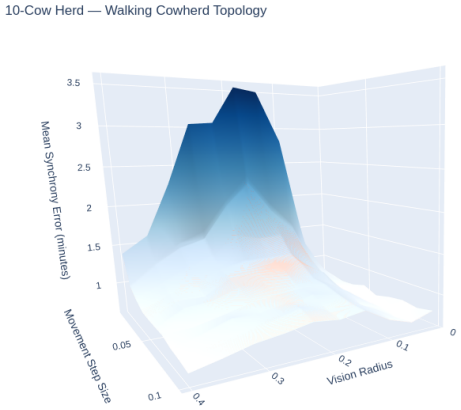

Figure 8: Synchronization error versus γ and ρ.

5 Conclusions

In this project, we explored a mathematical model that captures cows' individual and collective behavior using a hybrid dynamical system approach. We began with a single cow model to study how internal states, specifically hunger and fatigue, evolve continuously over time and lead to behavioral changes when certain thresholds are reached. By analyzing the return map and categorizing all possible transitions, we identified fixed points and multiple types of periodic orbits, providing a better understanding of the model's internal structure.

We then extended this model to a coupled setting, where cows influence each other through observable behaviors. Our simulations showed that even weak coupling can significantly enhance synchronization among cows, with stronger coupling and denser network structures leading to more pronounced alignment. This finding was stable across variations in parameter mismatches, network topologies, and even dynamic walking behavior in spatial simulations.

Overall, this model demonstrates how local interactions and simple switching rules can lead to emergent coordination in biological systems. It also highlights the power of combining differential equations, network theory, and hybrid system analysis to understand real-world phenomena. Beyond cows, this framework could apply to broader contexts in animal behavior, robotics, and distributed decision-making systems.

Our work makes the original paper by Sun et al. more accessible by breaking down key dynamics and simulating the model in a range of settings. The combination of mathematical analysis and computational experiments helped us deepen our understanding of how synchronization arises from individual rules and how mathematics can explain surprisingly coordinated behavior in natural systems. All simulation code, data, and additional visualizations used in this study are available at our project repository [1].

References

[1] A. Khurana and Collaborators. Apma 1360 final project: Cow synchronization models. https://github.com/brown-afkhurana/apma1360-final, 2025.

[2] Zihan Sun and Philip Holmes. Synchronization of cows: Evidence of emergent coordination in a hybrid system. *Physical Review E*, 106(4):044203, 2022.